UCRL-52881

SAFETY MARGINS ASSOCIATED WITH CONTAINMENT STRUCTURES UNDER DYNAMIC LOADING

Stephen C. Lu

October 30, 1978

This work was supported by the U.S. Nuclear Regulatory Commission under Interagency Agreement DOE 40-550-75 with the U.S. Department of Energy.

LAWRENCE LIVERMORE LABORATORY
University of California/Livermore

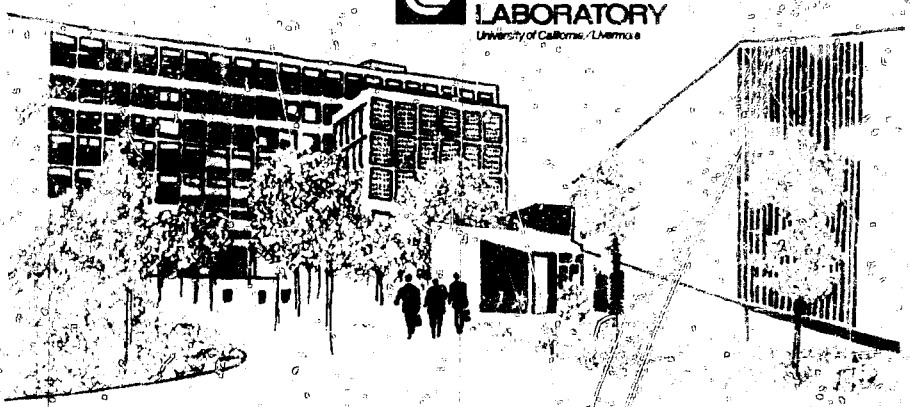

LAWRENCE LIVERMORE LABORATORY
University of California/Livermore, California/94550

UCRL-52581

SAFETY MARGINS ASSOCIATED WITH CONTAINMENT STRUCTURES UNDER DYNAMIC LOADING

Stephen C. Lu

MS. date: October 30, 1978

FOREWORD

This final report summarizes the results of a technical assistance program funded by the Engineering Branch, Division of Operating Reactors, Office of Nuclear Reactor Regulation, U.S. Nuclear Regulatory Commission. The program was originally funded in FY 77 (B&R 20100402 FIN A0208) and then continued in FY 78 as one of the tasks defined in the Engineering Mechanics Technical Support Program (B&R 20190403 FIN A0221). The purpose of the program is to provide the NRC with a technical basis for assessing the true safety margins of containment structures involved with MARK I boiling water reactor reevaluation activities. This report includes results of both FY 77 and FY 78, although FY 77 results were presented in a previously published paper.

The author thanks F. J. Tokarz of the Lawrence Livermore Laboratory and B. D. Liaw of the U.S. Nuclear Regulatory Commission for their continued interest in this work and for many helpful discussions.

CONTENTS

LIST OF ILLUSTRATIONS

LIST OF TABLES

ABSTRACT

A technical basis for assessing the true safety margins of containment structures involved with MARK I boiling water reactor reevaluation activities is presented. It is based on the results of a plane-strain, large displacement, elasto-plastic, finite-element analysis of a thin cylindrical shell subjected to external and internal pressure pulses. An analytical procedure is presented for estimating the ultimate load capacity of the thin shell structure, and subsequently, for quantifying the design margins of safety for the type of loads under consideration. For defining failure of structures, a finite strain failure criterion is derived that accounts for multiaxiality effects.

INTRODUCTION

The containment structures of nuclear power plants are designed to a large extent to satisfy the various stress limits specified in Subsection NE3000, Section III of the ASME Boiler and Pressure Vessel Code.[1] For rapidly applied, short-duration, dynamic loads, the common practice of meeting the Code stress limits based on a quasi-static approach is a poor measure of the reserve load-carrying capacity of a structure and always results in a conservative design with a superfluous margin of safety.

Normally this extra conservatism is acceptable although it may result in over-design of structures. There are situations, however, where quantifying this additional safety margin would avoid excessive or unnecessary field modification. Typical examples were found in reevaluation studies of MARK I Boiling Water Reactor (BWR) containment structures under the hydrodynamic loads expected during a postulated loss-of-coolant accident (LOCA).[2]

Both a short- and a long-term program were established by MARK I owners to resolve problems raised by these new hydrodynamic loads. Conservative load assumption, as well as analytical methods used in the short-term program, resulted in lower safety factors for containment structures than originally intended. The purpose of the long-term program is to restore the safety margins in the MARK I containments to those margins assumed to exist when these facilities were licensed.

Numerous experimental and analytical tasks are involved in the long-term program. The principal effort is to assess reasonably and realistically all phases of conservatism existing in load definition, design criteria, and in the analytical methods used in the short-term program. Subsequently, another load-definition report will be developed and distributed to the utilities for their use in final plant analyses.

The load-definition report and the structural and mechanical analyses will be reviewed by the staff of the U.S. Nuclear Regulatory Commission (NRC). To assist its overall evaluation of the adequacy of the long-term program, NRC has sponsored several efforts that parallel the long-term industry program. One is a program to determine the actual safety margins of containment structures when subjected to impulsive loads. This involves assessment of the true margins of safety as well as the design conservatism that would have existed when loads of short, finite duration were applied to structures designed to Code limits and in accordance with normal design practice. Some preliminary findings of the program were reported in a previous paper.[3] This report summarizes the final results.

APPROACH

To evaluate the true margin of safety of a containment structure subjected to rapidly applied dynamic loads, it is essential to determine the ultimate load capacity of the structure. This usually requires some type of very sophisticated nonlinear, transient, dynamic structural analyses. The nonlinearities are introduced by elasto-plastic material characteristics and large deformation effects.

To determine the ultimate dynamic load-carrying capacity, a set of pressure pulses with the same load duration but different magnitudes of peak pressure will be considered in the nonlinear dynamic analysis. Increasing peak values are chosen until the structure fails. The highest load magnitude that does not cause failure of the structure will be regarded as the ultimate load. Undoubtedly, this type of structural analysis can only be accomplished by executing a finite-element computer simulation. MARC[4] was judged the most suitable computer program for this investigation.

The typical containment structures investigated here are the wetwell torus shell and the vent-header structure inside the wetwell. The basic configuration for both types of structure is represented by a toroidal shell of circular cross-section that is supported radially at discrete locations. A realistic representation of the structural configuration would be a three-dimensional finite-element model that consists of a suitable number of two-parameter, curved-shell elements. However, it is generally considered a formidable task to conduct the series of nonlinear, transient dynamic analyses for such a three-dimensional finite-element model. To demonstrate the feasibility of the proposed approach and to obtain certain preliminary results, a reasonably simplified two-dimensional plane-strain model has been used in this program.

The basic structural difference between the vent-header and the wetwell shell, aside form their sizes, involves the type of loading acting on the structures. The wetwell torus shell is subjected mainly to internal pressure while the vent-header structure is predominantly under the action of impulsive, external pressure that is distributed nonuniformly on a portion of the exterior surface.

In addition to the series of dynamic analyses, a quasi-static analysis with the same pressure distribution is also included. The purpose is to demonstrate the distinct nature of the dynamic structural response as compared with a quasi-static approach. Subsequently, the true safety margin of the structure will be quantified, once the ultimate load is determined by the dynamic analysis.

FAILURE CRITERIA

Failure criteria are needed to determine the ultimate load-carrying capacity of the structure as defined. The choice of failure criteria depends on types of structures and types of loading conditions. For thin-shell structures subjected to internal or external pressure, two general failure modes are expected, i.e., the material-failure mode and the buckling-failure mode.

For structures under quasi-static loads, the distinction between the two types of failure modes is clear. Under slowly increasing internal pressure, a thin-shell structure deforms gradually until the deformation is so large that material rupture appears in the shell and eventually causes the failure of the entire structure. While the material failure mode is a gradual process for ductile material, the buckling mode for quasi-static type of loading can be very abrupt. The buckling mode is characterized mathematically by the formation of nonpositive, definite structural stiffnesses and the suddenly undefined deformation of the structure.

A finite-element computer program can easily be designed to detect the buckling of a finite-element model by constantly examining the singularity of the stiffness matrix during a loading path. To detect the material-failure mode, a failure criterion must be incorporated into the finite-element computer program so that certain control variables can be constantly monitored.

The controls can include stress, strain, displacement, or some integrated energy quantity. The stress control would be difficult to apply to elasto-plastic materials, because stresses change little if any once yielding is reached. Displacement control seems to be arbitrary and requires a lot of intuitive engineering judgment unless it is specifically stated in the design requirements. The energy control is a reasonable way to measure the structural load capacity. However, the additional computations required can be considerable, especially for a nonlinear, transient analysis. Therefore, it is obvious that strain control represents the best choice.

In a simple tension test of a material, the uniaxial-failure strain is clearly defined after the stress-strain curve has been properly recorded during the loading procedure. The strain state in a real structure, however, is much more complicated and requires certain assumptions and justifications to extend the uniaxial-strain-failure theory to that of a multiaxial strain.

To account for large deformation effects, the true strain will be considered distinct from the usual engineering strain. For a simple-tension-test specimen with original length ℓ_o and deformed length ℓ, the usual engineering strain ε and the true strain e are defined respectively by

$$\varepsilon = (\ell - \ell_o) / \ell_o = \ell/\ell_o - 1 \tag{1}$$

and

$$e = \int_{x=\ell_o}^{x=\ell} \frac{dx}{x} = \ln(\ell/\ell_o) = \ln(1 + \varepsilon) \quad . \tag{2}$$

The true strain is also called the logarithmic strain and can further be decomposed into a true elastic strain e^E and a true plastic strain e^P such that

$$e = e^E + e^P \quad . \tag{3}$$

The true plastic strain e^P is defined by

$$e^P = \ln(\ell_p/\ell_o) \quad , \tag{4}$$

where ℓ_p is the length of the test specimen at an intermediate deformed state that accounts for all pure plastic deformation. Because elastic deformation is considered small, the true elastic strain e^E can be used interchangeably with the engineering elastic strain and is simply defined as

$$e^E = S/E \quad , \tag{5}$$

where S is the uniaxial stress at the deformed state and E is the Young's modulus.

For multiaxial strain states, the equivalent true strain $\bar{e}$ is defined as the sum of the equivalent, true plastic strain $\bar{e}^P$ and the equivalent, true elastic strain $\bar{e}^E$. The equivalent, true plastic strain can be calculated by integrating plastic flow over the entire deformation history, or,

$$\bar{e}^P = \int \left(\frac{2}{3} de^P_{ij} \, de^P_{ij} \right)^{1/2} , \tag{6}$$

where de^P_{ij} are the components of the incremental, plastic strain tensor $d\underset{\sim}{e}^P$ that defines the instantaneous plastic flow.[5] Noting that plastic flow is incompressible, we see that the equivalent, true plastic strain defined by eq. (6) reduces to the uniaxial true plastic strain expressed by eq. (4).

The equivalent, true elastic strain $\bar{e}^E$, which is small compared with $\bar{e}^P$, is loosely defined by

$$\bar{e}^E = \bar{S}/E , \tag{7}$$

where S is the equivalent Von Mises stress as usually defined.[6] Again, the equivalent true elastic strain defined by eq. (7) reduces to the uniaxial true elastic strain defined by eq. (5), because in a uniaxial stress state, the equivalent stress $\bar{S}$ is simply the uniaxial stress S.

Using the symbol e_u to indicate the uniaxial true strain at rupture, a strain-failure criterion can be proposed in the general form

$$\bar{e} \leq f(F) e_u \tag{8}$$

or

$$\bar{e}^P \leq f(F) e_u - \bar{S}/E , \tag{9}$$

where F is the inverse of the triaxiality factor TF and where f(F) indicates a certain function of F. Note that the true rupture strain e_u can be computed from the engineering rupture strain ε_u by this relationship:

$$e_u = \ln(1 + \varepsilon_u) \quad . \tag{10}$$

Following Davis and Connelly,[7] we define the triaxiality factor TF, and hence its inverse F, as

$$TF = 1/F = 3\, S_{mean}/\bar{S} \quad , \tag{11}$$

where S_{mean} is the mean value of the three principal stresses. The function f(F), which accounts for multiaxiality effects, can be chosen to suit any particular case, depending upon what test data are available. A power law in terms of F is conveniently suggested,

$$f(F) = F^n \quad . \tag{12}$$

Results of eq. (12) compared with the biaxial test results reported in Ref. 8 are shown in Fig. 1 for n = 0.5, 0.75, and 1. Whereas n = 1 was considered by Riccardella,[9] n = 0.75 is used in this paper.

Because of the effects of inertial terms introduced in the equations of motion for structures under dynamic loads, the distinction between the two types of failure modes is no longer clear. This is so even though thin-shell structures still respond differently to external than to internal pressure loads. The abrupt, unbounded deformation of structures observed in quasi-static responses does not usually occur in dynamic analyses.

One analytical explanation can be offered by considering the time-integration scheme used in a finite-element computer program, taking, for example, the implicit Houbolt method used in MARC. The matrix $\underline{K}^*$ that is decomposed in each time increment of the time-integration procedure is a combined expression

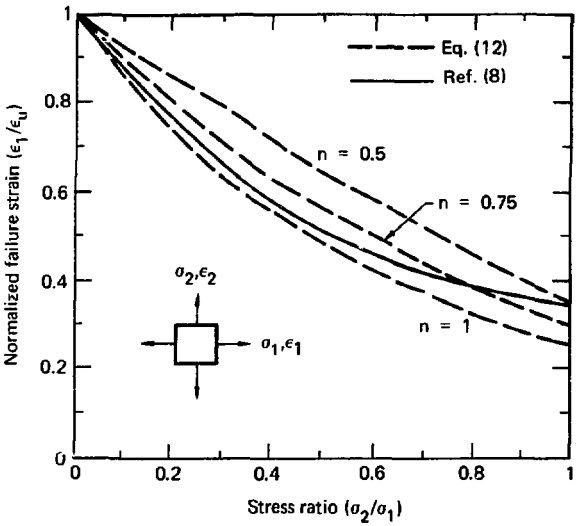

FIG. 1. Biaxial failure criteria.

of the stiffness matrix $\underline{K}$ and mass matrix $\underline{M}$; that is, $\underline{K}^* = \underline{K} + (2/\Delta t^2)\underline{M}$. Note that $\underline{K}$ can remain positive definite even though the stiffness matrix $\underline{K}$ has become singular. The reason is that the mass matrix of a structure usually stays positive definite throughout the load path.

Therefore, for both types of failure modes in dynamic analyses, the occurrence of structural failure is controlled by the strain-failure criterion discussed earlier. In other words, the unbounded deformation characterizing structural failure that results from either buckling or material rupture can be detected in a dynamic analysis only if the strain limit, defined by the failure criterion, is exceeded.

METHOD OF ANALYSIS

The large deformation, finite-element method is employed to perform the desired analyses. The finite-element computer program MARC is used for all numerical computations. MARC, or MARC-CDC, is a general purpose, finite-element computer program designed for linear or nonlinear and static or dynamic structural analyses. The program is written in FORTRAN IV computer language in a general form and with variable dimensions passed down to the subroutines. This program was modified to incorporate the strain-failure criterion described in the previous section. A user's subroutine also has been supplied to calculate the magnitude of the surface pressure at any integration point of an element and during each load increment of the analysis.

MARC has an extensive element library, which is capable of covering various types of structures ranging from simple trusses to sophisticated shell structures. The MARC type 15, isoparametric elements form the finite-element model for our problem. The element is a two-node, axi-symmetric, thin-shell element with four generalized nodal displacements at each node, i.e., two global displacements and their derivatives, chosen with respect to distance along the element. A cubic-displacement assumption is used to interpolate displacement field in terms of the generalized nodal displacements associated with the element. Element properties, including stiffness matrix, mass matrix, and generalized nodal-force vector, are computed by numerical integration. An 11-point Simpson rule is used through the shell thickness while a 5-point Gaussian integration is used along the element. The "ALL POINT" option in the computer program is capable of generating stress and strain output at all 55 points within the shell element.

The large displacement, elasto-plastic analysis is formulated in a series of piecewise, linear increments. The material behavior is assumed to be governed by the incremental theory of plasticity and the Von Mises yield criterion with an isotropic strain-hardening rule.

The incremental plastic-strain tensor $d\underset{\sim}{e}^P$ is given by the normal-flow rule of plasticity

$$d\underset{\sim}{e}^P = d\bar{e}^P \frac{\partial \bar{S}}{\partial \underset{\sim}{S}} \quad , \tag{13}$$

where $d\bar{e}^P$ is the equivalent incremental plastic strain that can be derived from eq. (6), and $\underset{\sim}{S}$ is the stress tensor.

The strain-hardening rule, in an incremental form, can be expressed by

$$d\bar{S} = H\, d\bar{e}^P \quad , \tag{14}$$

where H denotes the strain-hardening slope of the equivalent stress and equivalent plastic-strain curve obtained from a uniaxial test.

Because stresses depend only on elastic strains, we can write

$$d\underset{\sim}{S} = \underset{\sim}{D}\, d\underset{\sim}{e}^E \quad , \tag{15}$$

where $\underset{\sim}{D}$ is a material-property tensor denoting the usual linear elastic constants, and $d\underset{\sim}{e}^E$ is the incremental elastic-strain tensor.[4] For small elastic deformation, the total incremental-strain tensor $d\underset{\sim}{e}$ is

$$d\underset{\sim}{e} = d\underset{\sim}{e}^E + d\underset{\sim}{e}^P \quad . \tag{16}$$

After some manipulation, we obtain the following incremental elasto-plastic stress-strain relation:

$$d\underset{\sim}{S} = \underset{\sim}{D}' d\underset{\sim}{e} \quad . \tag{17}$$

The tensor $\underline{D}'$, which characterizes the instantaneous elasto-plastic material property, can be expressed in the following component form:

$$D'_{ijkl} = D_{ijkl} - \frac{D_{ijmn}\left(\frac{\partial \bar{S}}{\partial S}\right)_{mn}\left(\frac{\partial \bar{S}}{\partial S}\right)_{pq} D_{pqkl}}{H + \left(\frac{\partial \bar{S}}{\partial S}\right)_{mn} D_{mnpq}\left(\frac{\partial \bar{S}}{\partial S}\right)_{pq}} \quad . \tag{18}$$

Exercise of standard finite-element procedure[10] finally results in the following equation of motion:

$$\underline{M}\,\ddot{\underline{u}}(t) + \underline{I}(t) = \underline{P}(t) \quad , \tag{19}$$

where $\underline{M}$ is the mass matrix, $\ddot{\underline{u}}$ the generalized nodal-displacement vector, $\underline{I}$ the internal-force vector, $\underline{P}$ the external-force vector, and t the current time. The nonlinear ordinary differential equations expressed by eq. (19) can be solved by either an implicit or an explicit numerical integration scheme. If Houbolt's implicit integration method is used, we are required to solve, at each time increment, the following simultaneous equations in terms of the incremental displacement vector $\Delta\underline{u}(t)$, i.e.,

$$\left[\underline{K}(t) + \frac{2}{\Delta t^2}\underline{M}\right]\Delta\underline{u}(t) = \underline{P}(t + \Delta t) - \underline{I}(t) + \frac{\underline{M}}{\Delta t^2}\left[3\,\underline{u}(t) - 4\underline{u}(t - \Delta t)\right] + \underline{u}(t - 2\,\Delta t) \quad , \tag{20}$$

where Δt is the time increment and $\underline{K}(t)$ is the instantaneous stiffness matrix defined by

$$\underline{K}(t) = \frac{\partial \underline{I}}{\partial \underline{u}}(t) \quad . \tag{21}$$

The new displacement vector at $t + \Delta t$, therefore, is obtained as follows:

$$\underline{u}(t + \Delta t) = \underline{u}(t) + \Delta\underline{u}(t) \quad . \tag{22}$$

ANALYTICAL RESULTS

The structure under consideration is a long cylindrical shell, 54 in. in diameter and 0.25 in. thick. The dimensions of the structure are chosen to be compatible with a typical MARK I suppression pool, vent-header design. The SA516-GR70 carbon steel used has the following properties: Young's modulus 3×10^7 psi; Poisson's ratio 0.3, yield strength 35,000 psi; ultimate strength 70,000 psi; and mass density 7.35×10^{-4} lb-s^2/in.^{4}.

The thin-shell structure is subjected to nonuniform external or internal pressure with a parabolic pulse shape (Fig. 2). The finite-element model, formed by MARC type 15 axisymmetric thin-shell elements, is shown in Fig. 3. A large value is added to all radial coordinates to simulate plane strain effects. Only one-half of the symmetrical structure is considered. Twelve shell elements and four springs are presented in the model. The springs are used to account for the beam stiffness that exists in the actual BWR MARK I containment structures.

Three numerical examples were solved for pulse durations of 5, 15, and 30 ms in the case of external pressure. Because of the large nonlinear deformation, the load must be applied incrementally during static failure analysis. We used a 0.5-psi increment of the maximum surface pressure. During the static analysis, a nonpositive, definite stiffness matrix was reached as the maximum external surface pressure was increased from 17.5 psi to 18.0 psi. Therefore, 17.5 psi is the ultimate failure load for the static case.

In performing the dynamic analysis for each chosen peak pressure, a numerical time-integration scheme is required to obtain the transient structural responses. Both implicit and explicit integration schemes are available in MARC. The implicit Houbolt operator is used in the dynamic analysis. For each chosen peak pressure that does not exceed the failure pressure, a

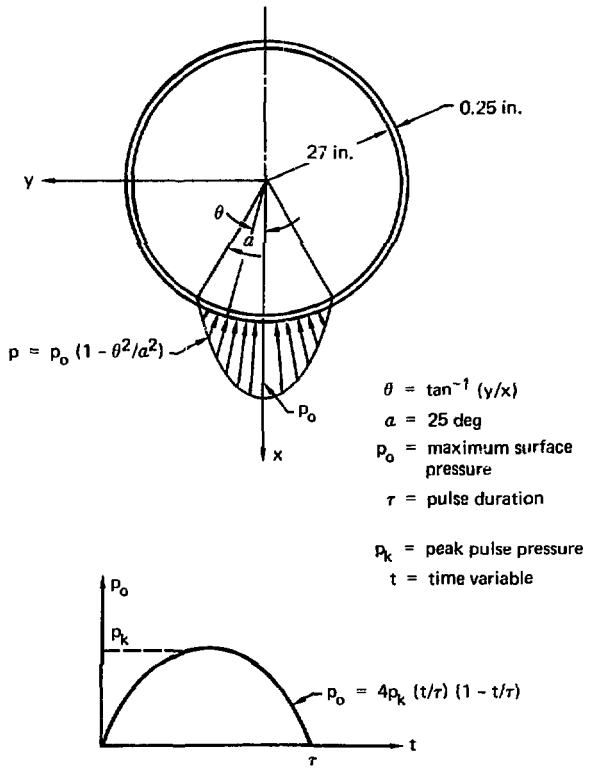

FIG. 2. Loading conditions.

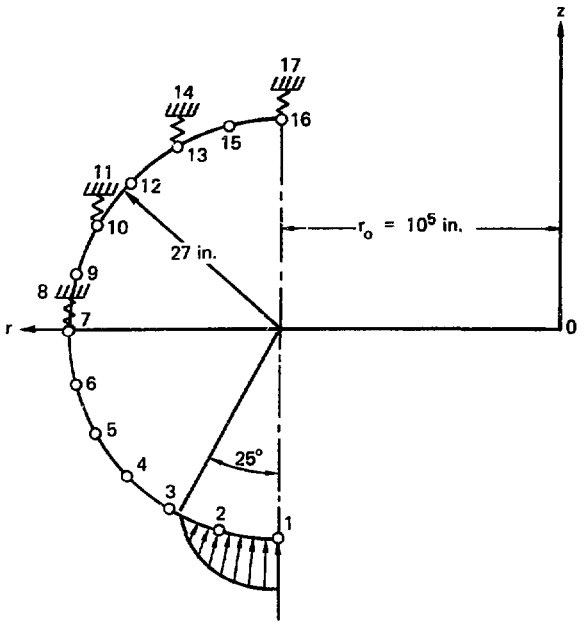

FIG. 3. Finite element model.

converged bounded solution can be achieved. In other words, the displacement of the shell increases with time, reaches a maximum value, and then decreases. If the chosen peak pressure is greater than the critical value, the displacement tends to go unbounded and will not reach a finite maximum. The time increment used in the dynamic analyses is 0.2 ms.

For pulse durations of 15 ms, dynamic analyses were performed for peak pressures of 5, 10, 15, 20, 30, 35, and 37 psi. The associated, transient structural responses are shown in Fig. 4. Converged solutions were obtained up to 35 psi. At 37 psi, failure of the structure was detected, and 35 psi

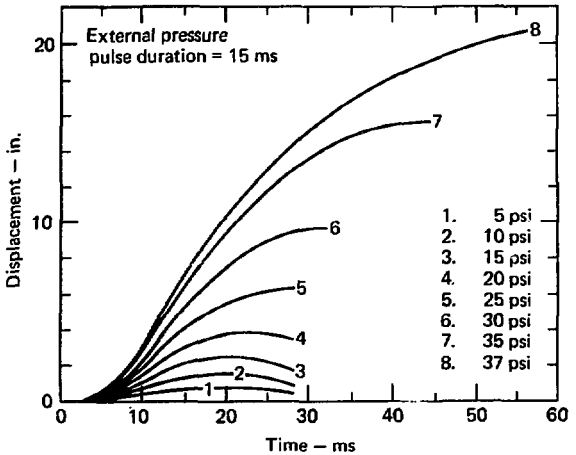

FIG. 4. Transient responses at node 1.

was then chosen as the dynamic failure load for this load case. The dynamic analyses were repeated for the other two cases. The ultimate loads were determined to be 90 psi and 20 psi, respectively, for load durations of 5 and 30 ms. As indicated by Fig. 5, the dynamic ultimate loads decrease asymptotically to the static value with increasing load durations.

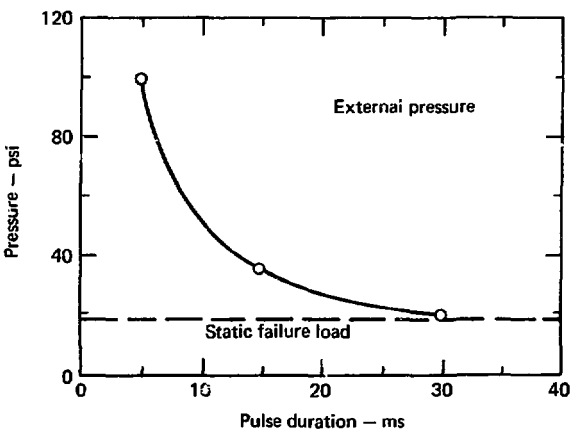

FIG. 5. Ultimate load vs pulse duration.

The results of both the static and the dynamic analyses of external pressure are summarized by Tables 1, 2, and 3 as well as Figs. 6 through 10.

TABLE 1. Displacement at node 1. (External pressure, 15-ms load duration)

P_o (psi)	Static displacement (in.)	Dynamic Displacement (in.)
0	0	0
2.5	0.344	-
5.0	0.716	0.740
7.5	1.117	-
10.0	1.572	1.532
12.5	2.288	-
15.0	3.648	2.468
17.5	5.806	-
20.0	∞	3.866
25.0	∞	6.252
30.0	∞	9.623
35.0	∞	15.570
37.0	∞	∞
40.0	∞	∞

TABLE 2. Stresses and strains at bottom shell surface for static analysis. (External pressure)

Maximum pressure (psi)	Hoop stress (psi)	Long stress (psi)	Hoop strain (%)	Equiv. stress (psi)	Equiv. strain (%)	Stress intensity (psi)
2.5	-11,680	-3,500	-0.035	10,380	0.035	11,680
5.0	-24,270	-7,280	-0.074	21,570	0.072	24,270
7.5	-37,740	-11,320	-0.115	33,540	0.112	37,740
10.0	-40,430	-15,140	-0.169	35,380	0.169	40,430
12.5	-42,040	-19,680	-0.307	36,440	0.320	42,040
15.0	-48,870	-22,210	-0.616	38,860	0.665	44,870
17.5	-48,570	-24,060	-1.022	42,060	1.003	48,570

TABLE 3. Stresses and strains at bottom shell surface for dynamic analysis. (External pressure, 15-ms load duration)

Maximum pressure (psi)	Hoop stress (psi)	Long stress (psi)	Hoop strain (%)	Equiv. stress (psi)	Equiv. strain (%)	Stress intensity (psi)
5	-19,370	-5,810	-0.059	17,220	0.057	19,370
10	-39,410	-11,900	-0.121	35,010	0.118	39,410
15	-41,090	-17,190	-0.219	35,750	0.223	41,090
20	-43,460	-21,210	-0.462	37,640	0.492	43,460
25	-47,320	-23,440	-0.885	40,980	0.966	47,320
30	-48,500	-24,030	-1.015	42,000	1.111	48,500
35	-52,790	-26,150	-1.486	45,720	1.639	52,790

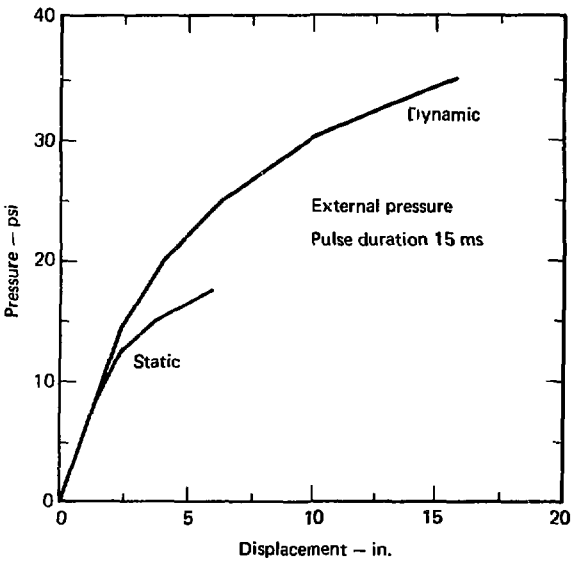

FIG. 6. Load vs displacement at node 1.

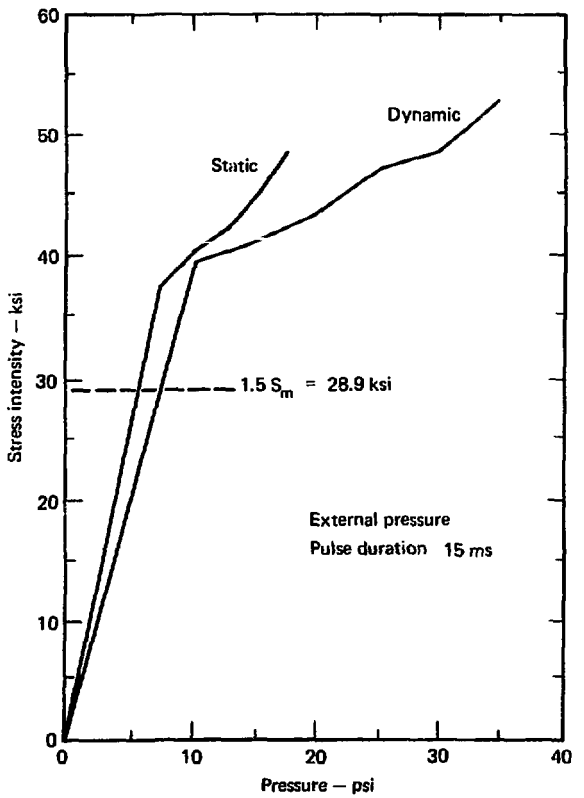

FIG. 7. Stress intensities in element 1.

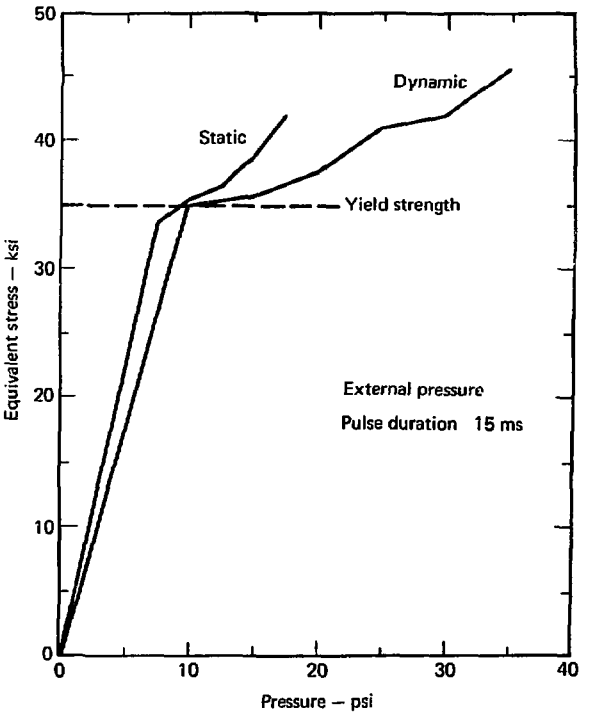

FIG. 8. Equivalent stress vs pressure.

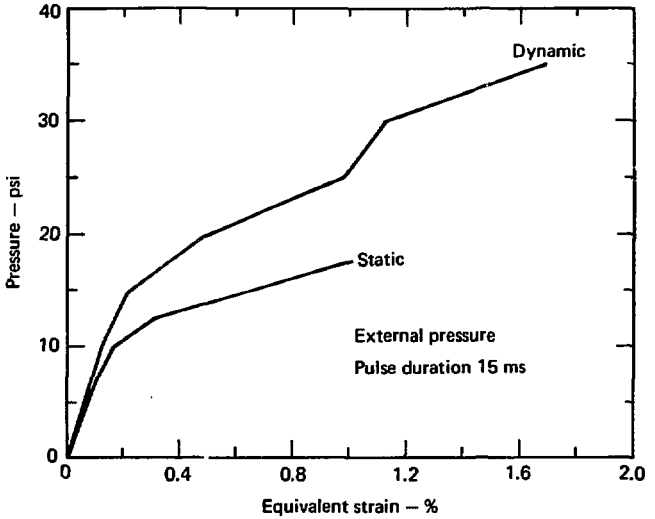

FIG. 9. Equivalent strain vs pressure.

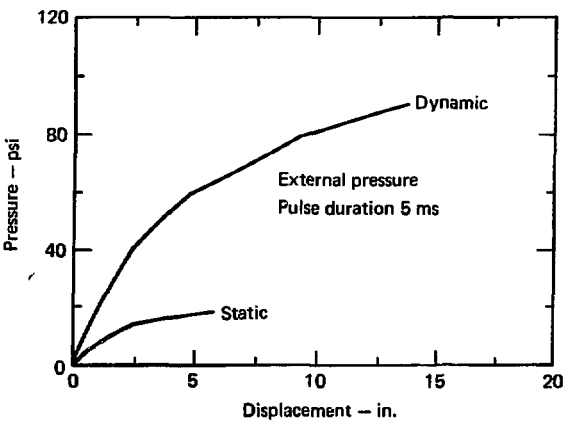

FIG. 10. Load vs displacement at node 1.

Similarly, the static and the dynamic analyses were also conducted for internal pressure of load duration 15 ms. The ultimate loads were 32 psi and 60 psi respectively for the static and the dynamic analyses. Tables 4, 5, and 6 along with Figs. 11 through 15 summarize the analytical results. As expected, the ultimate loads are considerably higher than those associated with external pressure.

TABLE 4. Displacement at node 1. (Internal pressure, 15-ms load duration)

P_o (psi)	Static displacement (in.)	Dynamic Displacement (in.)
0	0.	0.
5	.638	-
10	1.220	1.347
15	1.833	-
20	2.609	2.675
25	3.599	-
30	5.093	4.249
32	5.712	-
40	∞	6.435
50	∞	8.230
60	∞	9.075
70	∞	∞

TABLE 5. Stresses and strains at bottom shell surface for static analysis. (Internal pressure)

Maximum pressure (psi)	Hoop stress (psi)	Long stress (psi)	Hoop strain (%)	Equiv. stress (psi)	Equiv. strain (%)	Stress intensity (psi)
5	21,780	6,540	0.066	19,360	0.065	21,780
10	39,570	12,400	0.127	35,060	0.125	39,570
15	41,010	16,970	0.211	35,690	0.217	41,010
20	42,240	19,840	0.329	36,600	0.349	42,240
25	43,690	21,410	0.486	37,840	0.529	43,690
30	45,540	22,530	0.689	39,440	0.762	45,540

TABLE 6. Stresses and strains at bottom shell surface for dynamic analysis. (Internal pressure, 15-ms load duration)

Maximum pressure (psi)	Hoop stress (psi)	Long stress (psi)	Hoop strain (%)	Equiv. stress (psi)	Equiv. strain (%)	Stress intensity (psi)
10	36,310	10,890	0.110	32,280	0.108	36,310
20	41,390	18,090	0.248	35,940	0.258	41,390
30	42,830	20,840	0.428	37,090	0.463	42,830
40	44,850	22,140	0.614	38,850	0.675	44,850
50	46,560	23,130	0.838	40,330	0.933	46,560
60	52,620	26,310	1.598	45,570	1.805	52,620

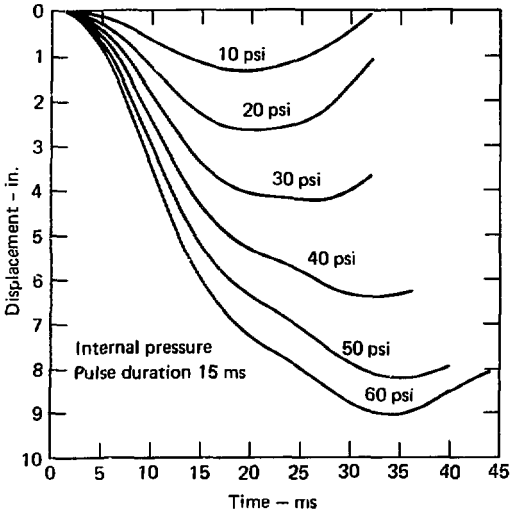

FIG. 11. Transient response at node 1.

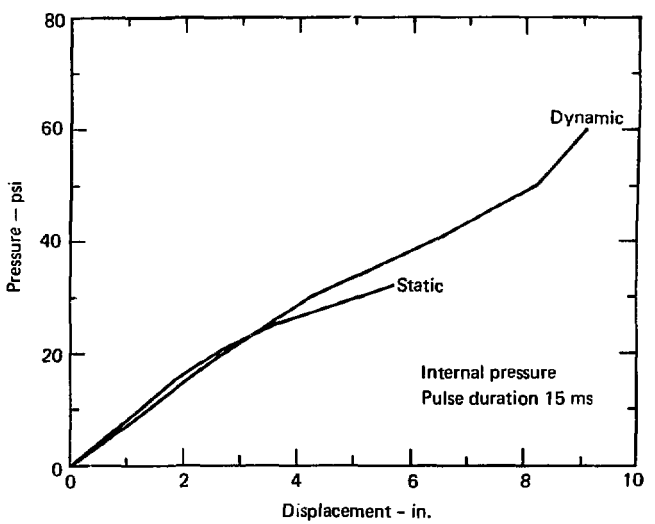

FIG. 12. Load vs displacement at node 1.

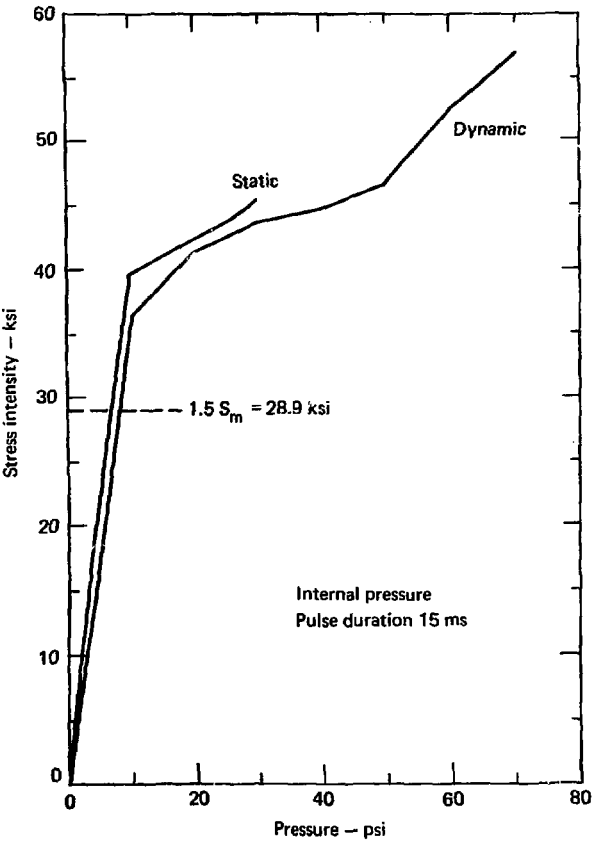

FIG. 13. Stress intensity vs pressure.

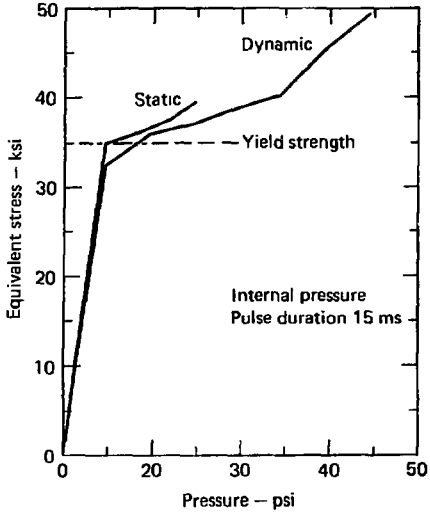

FIG. 14. Equivalent stress vs pressure.

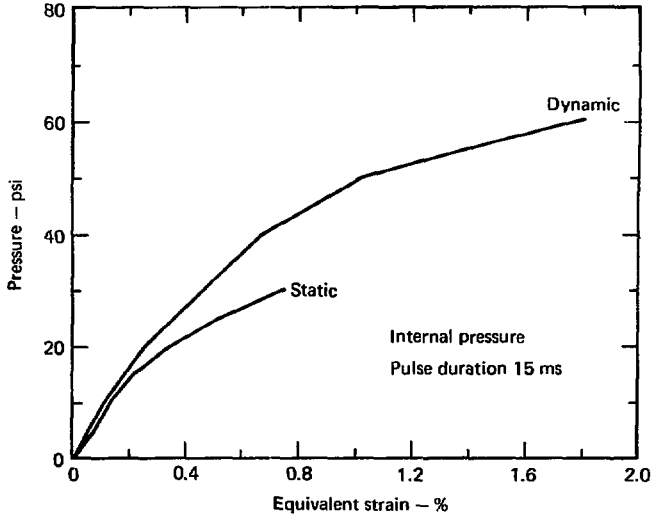

FIG. 15. Equivalent strain vs pressure.

INTERPRETATION OF RESULTS

Figure 6 clearly demonstrates the additional margin of safety that is associated with impulsive loading and that is not recognized in a quasi-static approach. The dynamic analysis in this case resulted in a failure load approximately twice that of the quasi-static analysis. To quantify the conservatism associated with the quasi-static approach, allowable loads were calculated for both the static and dynamic approaches, based upon requirements specified by the ASME Boiler and Pressure Vessel Code.

Two fundamental requirements are specified, either explicitly or implicitly, by the ASME Code. While the Code explicitly demands that stress intensities calculated from stress analyses should not exceed specific limits, it also tacitly requires that certain intended safety factors be provided by an acceptable structural design. The Code-intended safety factor, which we indeed can have in a simple tension situation, is obtained by comparing the ultimate material strength with the basic stress-intensity limit S_m. For MC components governed by Subsection NE, Section III, of the Code, the Code limits will yield an approximate factor of safety of 3.6.

Figure 7 shows stress intensities at different pressure levels for both the static and dynamic analyses. Because these are primary membrane plus bending stresses, the stress-intensity limit specified by the Code is 1.5 S_m, where S_m = 19.25 ksi for SA516-GR70 carbon steel. For the quasi-static analysis, the stress limit of the Code leads to an allowable load of 6 psi, which bears a safety factor of 2.9 against the static-failure load of 17.5 psi. Because the safety factor of 2.9 is less than the Code-intended safety factor of 3.6, the allowable load based on the static result is 4.9 psi.

On the other hand, if the dynamic result is used, the allowable load can be increased to 7.5 psi according to the stress intensity limit of 1.5 S_m. This would still provide a safety factor of 4.7 against the true ultimate load of 35 psi determined by the dynamic approach.

We now see that not only is the static allowable load of 4.9 psi conservative but the safety factor of 3.6, assumed to be provided by this load, is misleading. The true margin of safety provided by the 4.9-psi static allowable load is actually represented by a safety factor of 7.1, if it is appropriately evaluated according to the true ultimate load of 35 psi. Dividing the safety factor 7.1 (from quasi-static allowable load) by the factor 4.7 (from the dynamic result), we obtain a conservatism factor of 1.51 for the quasi-static approach over the dynamic analysis.

Both safety factors, 7.1 and 4.7, are greater, however, than the Code-intended safety factor of 3.6. Thus, we have discovered another type of conservatism, which is associated with Code stress limits. If the safety factor of 3.6 is to be achieved by an optimum containment structural design, the dynamic allowable load computed in this example represents a factor of conservatism of 1.31, i.e., the ratio of the dynamic safety factor of 4.7 divided by the Code-intended safety factor of 3.6. Similarly, an overall factor of conservatism of 1.97 is obtained for the static allowable load.

For a shorter load duration of 5 ms, an even more drastic increase in allowable load can be identified as shown in Fig. 10. In this case, the allowable load consistent with Code stress limits was 23 psi, according to the results of the dynamic analysis. The corresponding safety factor of 3.9 is clearly more appropriate than the factor of 18.4, which is associated with the quasi-static allowable load of 4.9 psi. Factors of conservatism of 4.72, 1.08, and 5.11 are obtained respectively for the quasi-static approach over the dynamic method and for the dynamic and static allowable loads, both with regard to the Code-intended safety factor.

The additional safety margin associated with impulsive loading is again depicted in Fig. 12 for the structure subjected to internal pressure. The static and dynamic Code-allowable loads were found to be 7.0 psi and 8.0 psi, which yielded safety factors of 8.57 and 7.50, respectively, according to the ultimate load 60 psi obtained in the dynamic analysis. Conservatism associated with the quasi-static approach (as against the dynamic method) and the static and dynamic allowable loads (with regard to the Code-intended

safety factor) can be quantified by conservatism factors of 1.14, 2.08, and 2.38. The result suggests an appreciable degree of conservatism in the Code stress limits.

In determining failure loads of structures by dynamic analyses, we used an artificially low value for uniaxial failure strain in eqs. (8) or (9), expressions of the proposed strain-failure criterion. A value of 0.05 was used, although the available stress-strain curve indicates a value of approximately 0.15 as the stress reaches the ultimate strength.

Our main reason for using the lower value, in addition to providing a safety margin to cover some uncertainty in the proposed failure criterion, was to shorten the time-history analysis as the finite-element model approaches a failure stage, thereby saving computer time. Instead of waiting for the strain in a failure-bound structure to hit a higher limit, we stopped the analysis earlier as the strain reached a reasonable limit.

In this procedure, the strength or the energy-absorbing capacity of material beyond the strain limit set in the computer code is neglected. Therefore, in certain cases the true failure of structures possibly may not occur even though the strain limit has been exceeded. In such a case, the calculated ultimate load theoretically would represent either a pseudo-solution or one of the lower bounds of the ultimate load. In other words, the ultimate loads so determined are believed to be conservative values.

CONCLUSIONS

A finite-element analytical procedure, along with a proposed failure criterion, has been presented for determination of ultimate loads of containment structures that are subjected to short-duration impulsive loads. The proposed procedure is needed for containment structures when identification of additional margins of safety is necessary to avoid unnecessary field modifications. Typical examples of this situation are found with BWR MARK I containment structures under pool-swell, hydrodynamic loads that follow a postulated LOCA.

The feasibility of the methodology has been demonstrated by the numerical examples discussed in this report. In these examples, additional margins of safety have been realized and quantified. The magnitude of safety margins provided by a structure is strongly dependent of the pulse durations of the applied dynamic loads, as shown by Fig. 5.

To realize fully the extra margins demonstrated in this report, a systematic parametric study involving dynamic loading characteristics, such as different load durations, pulse shapes, pressure distributions, and the like, should provide many useful guidelines for future containment structure design. Finally, to evaluate the true safety margins of containment structures at a specific nuclear power plant, an analysis which takes into account the three-dimensional configuration of the plant and its containment loading conditions is recommended.

REFERENCES

1. ASME Boiler and Pressure Vessel Code, Section III, Division 1, American Society of Mechanical Engineers, "Rules for Construction of Nuclear Power Plant Components, Subsection NE, Class MC components."
2. R. J. Stuart, "Structural Consideration - BWR MARK I Pool Dynamics," presented at the Fourth International Conference on Structural Mechanics in Reactor Technology, San Francisco, Calif., August 1977.
3. S. C. H. Lu, "Safety Margins of Containment Structures Under Impulsive Loading," presented at the 1978 Pressure Vessels and Piping Conference, Montreal, Canada, June 25-29, 1978.
4. MARC-CDC Nonlinear Finite Element Analysis Program, Control Data Corporation, Minneapolis, Minn.
5. S. C. H. Lu, "Incremental Stress Strain Relationship for Finite Elasto-Plastic Deformation," presented at the Second National Congress on Pressure Vessels & Piping, San Francisco, Calif., June 1975.
6. W. Prager, Introduction to Plasticity (Addison-Wesley, Reading, Mass., 1959).
7. E. A. Davis, and F. M. Connelly, "Stress Distribution and Plastic Deformation in Rotating Cylinders of Strain-Hardening Material," Journal of Applied Mechanics, Trans. ASME, 26 (1959), pp. 25-30.
8. W. E. Cooper, "Significance of the Tensile Test to Pressure Vessel Design," Welding Journal Research Supplement (Jan. 1957).
9. P. C. Riccardella, "Elasto-Plastic Analysis of Constrained Disk Burst Test," Journal of Engineering for Industry, Trans. ASME, 95, (Feb. 1973), pp. 129-136.
10. O. C. Zienkiewicz, Finite Element Method In Engineering Science, (McGraw-Hill, New York, 1971).

PM/jvb